Single-molecule imaging of von Willebrand factor reveals tension-dependent self-association

Running title: **Imaging tension-dependent VWF self-association**

Hongxia Fu[1-7], Yan Jiang[1,2,3], Wesley P. Wong[1,2,3], and Timothy A. Springer[1,2,3]*

[1]Program in Cellular and Molecular Medicine, Boston Children's Hospital, Boston, MA; [2]Department of Biological Chemistry and Molecular Pharmacology, Harvard Medical School, Boston, MA;

[3]Department of Pediatrics, Harvard Medical School, Boston, MA; [4]Division of Hematology, Department of Medicine, University of Washington, Seattle, WA; [5]Institute for Stem Cell and Regeneration Medicine, University of Washington, Seattle, WA; [6]Department of Bioengineering, University of Washington, Seattle, WA; and [7]Bloodworks Northwest Research Institute, Seattle, WA

*Correspondence: Timothy A. Springer, Center for Life Sciences, Room 3103, Boston Children's Hospital, 3 Blackfan Circle, Boston, MA 02215; e-mail: springer@crystal.harvard.edu;
Co-correspondence: Wesley P. Wong, Center for Life Sciences, 3rd floor, Boston Children's Hospital, 3 Blackfan Circle, Boston, MA 02215; e-mail: wesley.wong@childrens.harvard.edu

Word counts for text: 4192
Word counts for abstract: 250
Figure count: 5
Reference count: 31

(Title page notes)
Hongxia Fu and Yan Jiang contributed equally to this study.

Key points:

- Hydrodynamic drag on tethered VWF induces elongation and imparts mechanical tension that activates binding of free VWF at a tension of 10 pN
- Decrease in flow and hence tension on tethered VWF reverses VWF self-association.

Abstract

~~Von Willebrand factor (VWF) is an ultra-long concatemeric protein required for platelet plug formation after arteriolar injury in hemostasis and a critical mediator of thrombosis. VWF molecules show flow-dependent binding not only to platelet GPIbα but also to other VWF molecules; however, little is known about the mechanism or the flow-dependence of VWF self-association. Using single-molecule fluorescence microscopy, we directly visualize the kinetics of VWF binding to surface-tethered single VWF concatemers in flow. We show that intermolecular VWF self-association requires elongation of tethered VWF. Hydrodynamic drag exerts tensile force on tethered, extended VWF that is maximal at the tether point and declines linearly to zero at the downstream, free end. VWF self-association increases with tension, reaches half maximum at a characteristic tension of ~ 10 pN, and plateaus above ~ 25 pN. Association is reversible because a sharp decrease in flow and hence tension results in rapid dissociation of bound VWF molecules. Tethered VWF molecules can recruit more than their own mass of VWF from the flow stream. Kinetics show that instead of accelerating, the rate of accumulation decreases with time, revealing an inherently self-limiting self-association mechanism. GPIbα binding and VWF self-association occur in the same region of high tension in tethered VWF concatemers; however, the half-maximal tension required for activation of GPIbα is higher, suggesting differences in molecular mechanisms. By increasing the kinetics of both VWF self-association and binding to GPIbα, tension in tethered VWF concatemers activates the formation of networks of multiple VWF concatemers and platelets in hemostasis.~~

Von Willebrand factor (VWF) is an ultra-long concatemeric protein important in hemostasis and thrombosis. VWF molecules can associate with other VWF molecules, but little is known about the mechanism. Hydrodynamic drag exerts tensile force on surface-tethered VWF that extends it and is maximal at the tether point and declines linearly to zero at the downstream, free end. Using single-molecule fluorescence microscopy, we directly visualize the kinetics of binding of free VWF in flow to surface-tethered single VWF molecules and show that self-association requires elongation of tethered VWF and that association increases with tension in tethered VWF, reaches half maximum at a characteristic tension of ~10 pN, and plateaus above ~ 25 pN. Association is reversible and hence noncovalent; a sharp decrease in shear flow results in rapid dissociation of bound VWF. Tethered, primary VWF molecules can recruit more than their own mass of secondary VWF from the flow stream. Kinetics show that instead of accelerating, the rate of accumulation decreases with time, revealing an inherently self-limiting self-association mechanism. We propose that this may be because multiple tether points between secondary and primary VWF result in lower tension on the secondary VWF, which shields more highly tensioned primary VWF from further association. GPIbα binding and VWF self-association occur in the same region of high tension in tethered VWF concatemers; however, the half-maximal tension required for activation of GPIbα is higher, suggesting differences in molecular mechanisms. These results have important implications for the mechanism of platelet plug formation in hemostasis and thrombosis.

Introduction

In the arterial circulation, the glycoprotein von Willebrand factor (VWF) is of central importance in hemostasis and thrombosis ~~by sensing changes in blood flow to bind to platelets, other VWF molecules, and vessel walls to form a plug[1–5]~~. VWF is biosynthesized as concatemers consisting of variable numbers of covalently-linked monomers[1,2]. VWF concatemers are transiently attached to the endothelial cell surface during secretion and then circulate in blood plasma and attach to the subendothelial matrix at sites of injury[1-5]. Surface-tethered VWF can be activated by elevated shear stress to bind the platelet membrane receptor GPIbα[6,7]. Surface-tethered VWF may also associate with circulating VWF, a process known as intermolecular self-association[8-14]. Association of circulating VWF not only amplifies the amount of tethered VWF available to bind GPIbα to support platelet adhesion[8], but also enhances platelet activation[12]. VWF self-association thus contributes to platelet adhesion and aggregation during thrombus formation and is an important therapeutic target for hemostasis and thrombosis[15,16].

Despite progress in understanding VWF self-association, the molecular mechanisms and force requirements for self-association remain unclear. While higher shear stress has been found to induce a greater amount of binding between circulating and surface-attached VWF[9], self-association has also been observed in static conditions[10]. We showed with single-molecule imaging that shear flow induces surface-tethered VWF to elongate from a compact to a linear form and at higher flow rates the mechanical tension within VWF increases sufficiently to bind GPIbα from the flow stream[6,7]. One possibility is that VWF elongation and mechanical tension also activate association to VWF in the flowstream, but direct evidence for this hypothesis is currently lacking.

To date, association between surface-attached and circulating VWF has been studied at the macroscopic level using bulk VWF preparations, yet such studies average the behavior of samples containing VWF concatemers of a wide range of sizes, each of which experiences a different force history[8-14]. Here, to achieve quantitative insights into the mechanism and force-dependence of VWF self-association, we have measured VWF self-association kinetics within elongated, tethered single VWF molecules and revealed their dependence on tension.

Methods

~~**Recombinant VWF and GPIbα.** Alexa Fluor 488- and biotin-labeled recombinant human VWF used for surface tethering was prepared as described[6]. For use in the fluid phase, recombinant human VWF was labeled with Alexa Fluor 647 and dialyzed to remove free fluorophore. Human GPIbα was conjugated with Alexa Fluor 647 as described previously[6,7,17].~~

~~**Dual-color total internal reflection fluorescence (TIRF) imaging and microfluidic system.** The microfluidic and fluorescence imaging system[6] was modified by adding a manual pressure regulator to control the baseline pressure of the flow system (Figure 1A).~~

~~**Experimental procedures.** A flow channel with a biotin-PEG-doped PEG surface was incubated at 21°C sequentially with blocking buffer containing BSA and casein, traptavidin, biotin- and Alexa Fluor 488-labeled VWF concatemers, and D-biotin with washes in between. Finally, an imaging buffer containing free VWF with or without specified additions was flowed through the channel at 21°C. Fluorescence images were collected using the flow sequences and imaging frame rates listed in Supplemental Tables 1 and 2.~~

~~**Data analysis.** Fluorescence images were analyzed using a custom-written MATLAB code described previously[6] to calculate the extension of tethered VWF, the mass of VWF molecules, the number of VWF monomers, and the number of bound VWF or GPIbα as a function of time. Tension along tethered VWF was estimated as described in [6] and divided into tension bins. From these data, the~~

~~kinetics of free VWF or GPIbα binding were analyzed for each tension bin in tethered VWF molecules at different shear stresses.~~

Recombinant VWF and GPIbα and flow system. Recombinant human VWF was labeled with Alexa Fluor 488 and biotin, purified using size exclusion chromatography, and attached to the wall of flow channels coated with PEG and PEG- biotin[6]. Recombinant human VWF or GPIbα for use in the flow stream were labeled with Alexa Fluor 647[6,7,17]. The microfluidic flow channel was mounted on a total internal reflection (TIRF) microscope (Figure 1A). VWF or GPIbα were introduced in nitrogen-pressurized vials at one end of the flow chamber at 80 dyn cm^{-2} and switched at the speed of sound without introducing flow rates spikes by automatically actuated, sequential changes in nitrogen pressure to achieve flow rates of 240, 80, 480, 80, and 960 dyn cm^{-2} at 21°C. Images with 0.007 to 0.008 s exposure times were acquired at frame rates of 0.2 to 2 s^{-1} designed to minimize photobleaching (Supplemental Tables 1 and 2).

Data analysis. Fluorescent images of multiple single tethered VWF molecules in each frame were analyzed using a custom-written MATLAB code[6]. Based on the contour and fluorescence intensity of primary tethered and secondary bound VWF or GPIbα molecules, standardized with the intensity of single Alexa Fluor 488 and 647 fluorophores, and Alexa Fluor stoichiometry of coupling to VWF or GPIbα, VWF extension, mass, monomer number, and GPIbα number were calculated in each frame of movies. Tension along tethered VWF was estimated by summing the drag force on all downstream VWF monomers, modeled as a string of VWF domain beads[6]. The kinetics of free VWF or GPIbα binding were analyzed for each tension bin in tethered VWF molecules at different shear stresses.

Details are in Supplemental Methods.

Data sharing statement. Data generated by this study are available upon request. DNA construct for recombinant GPIbα is available in Addgene.

Results

VWF self-association in shear flow

To study VWF self-association in flow, we tethered recombinant human VWF labeled with Alexa Fluor 488 and biotin to a flow chamber wall coated with traptavidin[6]. Alexa Fluor 647-labeled free VWF at a physiologically relevant concentration of 10 μg mL^{-1} [18] was then infused at a wall shear stress of 80 dyn cm^{-2} with air-pressure actuated switching to intervening periods of flow at 240, 480, and 960 dyn cm^{-2} (Figure 1A-B).

Dual-color TIRF microscopy showed that tethered VWF was elongated at 80 dyn cm^{-2}, elongated further at 240, 480, and 960 dyn cm^{-2}, and rapidly relaxed to a shorter length upon return to 80 dyn cm^{-2} (Figure 1B). Little free VWF bound to the elongated, tethered VWF at 80 or 240 dyn cm^{-2}; however, much more binding occurred at 480 and 960 dyn cm^{-2} (Figure 1B-C). Free VWF preferentially bound near the VWF tether point on the substrate and bound further downstream along the length of the tethered VWF molecule at 960 dyn cm^{-2} as compared to 480 dyn cm^{-2} (Figure 1B and D).

While ligand binding in stasis depends on diffusion for the encounter between the ligand and receptor, flow transports free VWF past tethered VWF and hence increases the encounter frequency. Therefore, we compared binding at 240, 480, and 960 dyn cm^{-2} as if it was completely transport-limited; i.e., we compared binding over time interval lengths that were inversely related to shear such that the same number of free VWF molecules had flowed past in each case (Figure 1C). Increasing shear stress nonetheless increased VWF binding to tethered VWF, showing that increased binding was not due to increased VWF transport. At 960 dyn cm^{-2}, the mass ratio of bound VWF to tethered VWF nearly equaled 1 (Figure 1C). Furthermore, the rate of binding increased with shear, as shown by comparing the slopes of the binding curves at 960, 480, and 240 dyn cm^{-2} (Figure 1C). These results suggest tension-dependent activation of binding of tethered VWF to VWF in the flow stream.

Shear dependence of free VWF binding to tethered VWF was further demonstrated by rapid dissociation of most of the bound VWF after decreasing the wall shear stress to 80 dyn cm^{-2} (Figure 1B-C). Fits assuming two populations of bound VWF molecules (double exponential decay) showed that most VWF molecules dissociated at a rate of ~0.8 s^{-1} and a smaller population dissociated at a slower rate of ~0.02 s^{-1} in the presence of 10 μg mL^{-1} free VWF (Figure 1E). About 4% of bound VWF did not dissociate after ~5 min. After initial binding of free VWF to tethered VWF, some bound molecules may become photodamaged. Therefore, the minor population of slowly dissociating molecules could be, at least in part, artificial.

Tension regulates VWF self-association

To further study the role of tension in VWF self-association, we measured binding kinetics as a function of tensile force within tethered VWF. At each point along a tethered VWF molecule, mechanical tension is approximately proportional to the number of monomers downstream on which hydrodynamic drag force is exerted. The drag force was estimated as 0.38 pN per monomer at 960 dyn cm^{-2} [6]. Hence, tensile force along the VWF spine is maximal at the tether point and decreases linearly to zero at the downstream end. The time trace of binding at 10 μg mL^{-1} free VWF in each tension bin (Figure 2A) was used to calculate binding kinetics (Fig. 2B). Only tethered VWF molecules that were long enough to include a 40-60 pN force bin at 960 dyn cm^{-2} were included in the tension-based data analysis. Over time, binding of free VWF adds extra drag force to the tethered VWF molecule and thus increases tensile force between the tether point and the point(s) at which free VWF binds. Uncertainties in the number and location of binding sites between the tethered and bound VWF molecules, as well as heterogeneity in the evolution of the tension profile among individual tethered VWF molecules, prevented us from precisely taking these factors into account in our calculations. Therefore, we used the initial tension profile in tethered VWF before binding of free VWF and analyzed binding rates within the initial time period of binding at each flow rate to minimize the effects of bound VWF on further VWF binding (Supplemental Methods).

We used two measures of free VWF binding to tethered VWF. Binding kinetics were measured in the initial linear regime of the first 10 seconds of the 35 second binding periods for 10 μg mL^{-1} free VWF at 960 dyn cm^{-2}. We also measured final binding density by averaging bound VWF monomer numbers/μm tethered VWF at 33-35 s. Both measures increased markedly between the 0-10 and the 20-30 pN force bins, i.e., from about 5 to 25 pN, and then plateaued between 25 and 50 pN (Figure 2A-C). To take a closer look at the force range below the plateau, we used 5 pN rather than 10 pN tension bins to analyze initial binding rates at 480 dyn cm^{-2} (Figure 2D). The rate was low at 0-5 pN, sharply increased between the 5-10 and the 15-20 pN bins, and plateaued at the 15-20 and 20-25 pN bins. This sigmoid trend matches a two-state model. Therefore, we fit our data to such a model in which a site in VWF that does not bind, or binds slowly, is activated by force to a site that binds rapidly and presumably with high affinity (Figure 2E-F). Fits to data at 480 and 960 dyn cm^{-2} gave maximal binding rates and f_{50} values within error of one another and agreement with simple interpolation from the results. The data at 480 dyn cm^{-2} showed more points at low force (the 0-5 and 5-10 pN bins) where binding was low and therefore better emphasized the high tension required to activate binding kinetics and resulted in a larger ΔG value. Although neither Δx or ΔG are well determined, they illustrate the range of possible values allowed by our data.

Complexities of VWF self-association

Accumulation of VWF in flow on tethered VWF has multiple complexities. VWF concatamers have many monomers, and thus binding may involve multivalent interactions between multiple monomers in both the tethered and bound VWF concatemers (Fig. 3A). Furthermore, once VWF in flow binds, it provides further, secondary VWF binding sites that increase the total tension on the primary

tethered VWF concatemer. However, if primary and secondary VWF bind to one another at multiple sites, few secondary VWF monomers would be downstream of each interaction site, limiting tension buildup on secondary VWF. At the same time, secondary VWF could block access to primary VWF and inhibit further accumulation (Fig. 3A).

These complexities were reflected in concentration-dependent VWF accumulation (Figure 3B). Over a range of VWF concentrations, accumulation at 480 and 960 dyn cm^{-2} was faster in the first half of the accumulation period than in the second half. This is an important observation, because if VWF accumulated from the flow stream was as effective as tethered VWF for the accumulation of further VWF, the rate of accumulation would accelerate, instead of slowing as observed. The slowing of the rate of binding is similar to what is observed in saturation binding; however, only a few monomers with force-activated binding sites within tethered VWF might suffice to bind VWF in flow and therefore saturation binding may not be the correct explanation. The ability of tethered VWF to bind more than its own mass of VWF is illustrated by binding after 35 s at 960 dyn cm^{-2} of 1.5 fold more mass from the flow stream at 50 μg mL^{-1} (Figure 3B).

To quantitatively examine these complexities, we studied accumulation at 960 dyn cm^{-2} with time as a function of both free VWF concentration and tension bin within the tethered VWF (Figure 4A, unbroken lines). The initial rate of binding and total accumulation increased as VWF concentration increased from 1 to 50 μg mL^{-1} in all tension bins (Figure 4A). At the highest tension bin of 40-60 pN, binding of VWF at 10 μg mL^{-1} was still increasing after 30 s and at 35 s reached 40.1±2.5 bound monomers/μm of tethered VWF; at 50 μg mL^{-1} of VWF, binding reached 77.5±0.9 bound monomers/μm at 35 s (Figure 4A). Binding in the 40-60 pN bin corresponded to bound/tethered VWF mass ratios of 1.1±0.1 and 2.00±0.02 at 10 and 50 μg mL^{-1}, respectively, and agrees with the ability of tethered VWF to bind more than its own mass of free VWF as shown in Figure 3.

The free VWF binding kinetics deviated from a simple homogeneous 1:1 binding model. Globally fitting our binding kinetics measurements in each tension bin and at each VWF concentration to such a model only partially matched the results (Figure 4A, dashed lines), likely due to the complexities discussed in this section.

Therefore, to minimize the effects of free VWF accumulation, we quantified the initial free VWF binding rate k_{obs} at the first 35, 20, and 10 seconds for 1, 5, and 10 μg mL^{-1} of free VWF, respectively. We omitted the binding rates at 50 μg mL^{-1} where the greatest amount of VWF accumulation occurred and fit k_{obs} to a linear function of free VWF concentration at 0 to 10 μg mL^{-1} (Figure 4B). Fitting to our experimental data yielded the force-dependent slope a(f). a(f) increased with tension and reached a plateau at $(5.8\pm1.3)\times10^{-14}$ mL μm^{-1} s^{-1} above 25 pN (Figure 4C). The value of the parameter a(f) plateaued in the 20-30 pN tension bin and above, and the f_{50} value of 11.5±0.6 pN (Figure 4C) was consistent with f_{50} values from other measurements (Figure 2).

Coexistence of VWF self-association and GPIbα binding

Since the VWF A1 domain binds platelet GPIbα and has also been implicated in VWF self-association[1,2,14], we examined the effects of VWF self-association on GPIbα binding and the effect of GPIbα binding on VWF self-association. We measured the binding of Alexa 647-labeled GPIbα to Alexa 488-labeled, tethered VWF in the presence of varying concentrations of unlabeled, free VWF at 960 dyn cm^{-2}. High-affinity GPIbα with G233V and M239V gain of function mutations found in patients with platelet-type von Willebrand disease was used to achieve a high signal-to-noise ratio[7,17]. The fluorescence intensity of bound GPIbα increased rapidly and plateaued after about 10 s of flow at 960 dyn cm^{-2} (Figure 5A). The binding of GPIbα was highly tension dependent, as previously described [6]. However, whether free VWF was present at 0, 10, or 50 μg mL^{-1}, it had little effect on GPIbα binding whether binding was measured at 1.5-2.5 s or 27-35 s (Figure 5B and C).

Conversely, we measured the binding of Alexa 647-labeled free VWF to Alexa 488-labeled tethered VWF in the presence of 200 nM unlabeled, high-affinity GPIbα, a concentration that is 33-fold higher than its ~6 nM Kd for mechanically tensioned VWF above 30 pN [7]. A small but significant amount of inhibition of VWF self-association was observed (Supplemental Figure 1). The ARC1172 aptamer binds to a site on A1 that overlaps with the GPIbα binding site ~~and~~on A1 and ARC1172 completely inhibits GPIbα binding [19,20]. ARC1172 at 60 nM, a concentration 100-fold higher than its 0.6 nM Kd for A1 [19] also modestly but significantly inhibited VWF self-association (Supplemental Figure 2). However, the ~~lack~~small amount of ~~complete~~ inhibition by ~~either competitor~~these competitors, despite their use at levels much higher than their Kd values, suggests that they ~~may be affecting~~affect self-association by a mechanism other than competing for the same binding site.

Discussion

Our measurements provide important insights into how circulating plasma VWF associates with VWF tethered to the blood vessel wall to regulate hemostasis and thrombosis. We reconstituted the process of VWF self-association on single tethered VWF concatemers in shear flow and directly measured the kinetics and the effect of tension on this process. To bind free VWF, we found that tethered VWF must not only elongate from a compact ~~to an extended form but also reach a tension of 10 pN for half maximal accumulation (the f_{50} value) (Figure 6).~~, random coil state[21] to an extended form but also reach a tension of 10 pN for half maximal accumulation (the f_{50} value). Accumulation plateaued at forces above 20 pN.

Flow applies a hydrodynamic force to tethered VWF molecules, inducing mechanical tension within them. The flow-induced mechanical tension is highest at the tether point and decreases linearly to zero at the downstream end of the tethered VWF concatemer. This tension distribution was reflected in the localized pattern of VWF binding from the flow stream. Tethered VWF was extended by shear flow in our basal condition of 80 dyn cm^{-2}, yet binding of free VWF was not detected. The binding was barely detectable at 240 dyn cm^{-2}, was marked at 480 dyn cm^{-2}, and greater at 960 dyn cm^{-2}. The latter two wall shear stresses are not found physiologically and are expected only to be present during excessive blood flow at sites of bleeding, especially with the vasoconstriction that accompanies vessel injury, or in pathologies including stenosis[6]. Alternatively, at physiologic shear stresses, binding of platelets to tethered VWF would increase mechanical tension and bring it into the range required for VWF self-association.

One tethered VWF concatemer could bind multiple concatemers from the flow stream. Tethered VWF molecules were observed to bind more than their own mass of VWF molecules from the flow stream, showing that self-association has the potential to amplify hemostasis and thrombosis. The multimeric nature of a VWF concatemer is important for it to bind multiple other concatemers, just as a single concatemer could bind multiple platelets. Multiple attachments might form between a primary and a bound (secondary) concatemer (Figure 3A). If so, this would minimize the tension in secondary VWF molecules, because only monomers between each attachment point would contribute tension to the upstream attachment point.

Theoretically, VWF bound from the flow stream (secondary VWF) could have the capability of binding further VWF (tertiary VWF). This would cause binding from the flow stream to accelerate; however, the opposite occurred, i.e., the rate of binding decreased. On the other hand, VWF binding also did not become saturated on our experimental time scale, even after accumulation of more than 1.5 times the mass of the tethered VWF. Saturation of binding sites may be one of the factors that slowed VWF accumulation, even though only a small proportion of VWF monomers in both concatemers may be required for binding. Another factor would be the limitation by multipoint binding of tensile force on secondary VWF, as discussed in the previous paragraph. While secondary, bound VWF would apply

additional tension to primary, tethered VWF, it would also partially shield it from binding further secondary VWF, and thus could contribute to the decrease in the rate of VWF binding (Fig. 3B).

In contrast to the small GPIbα ectodomain, substantial hydrodynamic force is applied to a secondary VWF concatemer, which could help break VWF self-association bonds. Thus, force-promoted dissociation may also contribute to slowing of accumulation described in the previous paragraph.

When flow was returned to our baseline 80 dyn cm^{-2} wall shear stress, most bound VWF rapidly dissociated from VWF tethers even though the tethers remained extended. ~~Similarly,~~ This finding emphasized that VWF self-association was noncovalent and completely distinct from the covalent disulfide bonds that link VWF monomers head-to-head and tail-to-tail into concatemers. Like VWF, GPIbα extracellular fragments also rapidly dissociated from tethered VWF when flow, and hence mechanical tension, were lowered below a threshold[6].

Tethered VWF may be found in vivo at vascular sites of stimulated secretion from endothelial cells or of damage that exposes subendothelial collagen for VWF binding. The average single VWF concatemers studied here were 3.6±1.1 μm in length at 960 dyn cm^{-2}. VWF tubules stored in Weibel-Palade bodies can be as long as 5 μm. Each is thought to contain a single VWF concatemer with a maximal extension of ~250 μm [2]. Therefore, as a VWF concatemer is being extruded during secretion, it could form a tether with a length much longer than studied here, with a correspondingly higher tension within it.

The A1 and A2 domains are known to be responsive to mechanical tension in VWF concatemers and are plausible binding sites in VWF self-association. Therefore, it is intriguing to compare the force requirements for VWF self-association found here with those previously found for VWF A1 domain binding to GPIb[6,22,23] and for A2 domain unfolding[24-26]. Most previous measurements differed from those here in being force ramp experiments, in which force was linearly increased until an event occurred. In contrast, here we have measured VWF binding frequencies as a function of a constant flow rate within bins of constant tension. Thus, the dependence on force of the equilibrium between active and inactive sites for self-association in the tethered VWF was measured here. As mechanical tension increased, the fraction of active sites increased from 0% to 100~~% and~~%; the f_{50} value ~~characterizes~~characterized when the fraction of active sites was 50%. Thus, the f_{50} value of 10 pN measured here for activation of the site(s) for self-association corresponds to the force at which the rates of activation and inactivation are equal. Reversibility was established by dissociation of secondary VWF when the flow rate was lowered to 80 dyn cm^{-2}. Among the previous measurements cited in this paragraph, only one is directly comparable, and showed that the equilibrium between binding and unbinding of GPIb to the A1 domain of VWF occurred with an f_{50} value of 20 pN [6]. The large difference from the f_{50} value of 10 pN for VWF self-association strongly suggests that GPIb binding and VWF binding are activated by distinct mechanisms. This is in agreement with the failure of GPIb and ARC1172 to have more than a modest effect on VWF self-association, which suggests that their binding sites do not overlap with the binding site for VWF self-association and that they may inhibit by an indirect mechanism such as binding to a nearby site.

A2 domain unfolding is difficult to compare to our f_{50} value because the peak of the force distribution for A2 unfolding was measured during force ramp experiments[24-26] and the peak force is proportional to the log of the rate of force increase[27,28] . The A2 domain appeared to be stabilized by its neighbors, because at a force ramp of 22 pN s^{-1}, it unfolded at 11 pN as an isolated A2 domain and at 22 and 23 pN in intact VWF and in $(A1A2A3)_3$ concatemers, respectively[24,25]. Refolding of isolated A2 occurred in ~3 s at 1 pN [24]. If A2 refolding also were stabilized by its A1 and A3 neighbors, then it might be possible that in intact VWF, the rates of A2 unfolding and refolding would be equal at ~10 pN,

as would be required for the unfolded A2 domain to be a candidate for the binding site for VWF self association. However, our experiments in shear flow (here and [6]) use an estimate of the force calculated from fluid dynamics rather than more direct measurements based on calibrations[24,25]. It will be important to test A2, as well as other domains in VWF, as possible sites for self-association in the primary VWF concatemer. It also is important to define the binding site(s) in the secondary VWF concatemer for self-association.

The ability of mechanical tension to activate VWF binding shows that the active state is more extended than the inactive state, which would be the case for the unfolded A2 domain, and also for other mechanically sensitive domains that have high affinity folded states that are more extended than low affinity folded states[29-31].

Our direct measurements here of VWF self-association in shear flow allow this process to be understood more fully in the overall process of formation of the VWF-platelet plug in vivo. The force-dependent unfolding of the A2 domain exposes tethered VWF to cleavage by the protease ADAMTS13, which would liberate VWF fragments downstream of the cleavage site into the flow stream and also decrease the tension on the remaining upstream fragment. In contrast, binding of platelets and VWF in the flow stream to tethered VWF increases tension on the tethered VWF. Furthermore, our finding that VWF binding from the flow stream did not accelerate further accumulation of VWF suggests an inherent feature in VWF that limits its self-association and prevents an uncontrolled chain reaction even in the absence of physiological regulation such as by ADAMTS13 cleavage.

Previously, shear-dependent VWF self-association has been investigated in complex systems involving platelet-VWF as well as VWF-VWF interactions and interactions in whole blood[8-14]. The single-molecule assay developed here goes to the heart of VWF self-association by probing the VWF-VWF interaction directly and has revealed its dependence on mechanical tension within tethered VWF, association kinetics, and reversal when mechanical tension is lowered. The similar yet distinct ranges of the tensions required for self-association, activation of the high-affinity state of VWF A1 for GPIbα, and unfolding of A2 for cleavage by ADAMTS13 allow hemostasis and thrombosis to be exquisitely sensitive to rapid changes in blood flow at a site of hemostasis or thrombosis. However, much more remains to be learned about the identity of domains in tethered VWF and VWF in the flow stream that associate with one another and the mechanism by which tension induces binding, presumably by stabilizing a more extended conformation of a domain within VWF. Since VWF is multimeric, it is possible that self-association involves contacts between multiple monomers in each concatemer. Finally, it will be important to find agents that completely inhibit self-association to better define its molecular mechanism and to test as therapeutics in thrombosis.

Acknowledgements

We acknowledge help from the microfluidic prototyping facilities at the Wyss Institute for Biologically Inspired Engineering at Harvard. This work was supported by NIH NHLBI K25HL135432 (H.F.), ASH Scholar Award (H.F.), NIH NHLBI K25HL146949 (Y.J.), NIH NIGMS R35 GM119537 (W.W), and NIH HLBI R01HL148755 (T.A.S.)

Authorship Contributions

T.A.S., W.P.W., H.F., and Y.J. designed the research and drafted the manuscript. H.F. and Y.J. performed the experiments. T.A.S., W.P.W., H.F., and Y.J. analyzed data.

Conflict-of-interest Disclosure: All the authors declare no competing financial interests.

ORCID profiles: H.F., 0000-0002-6893-8260; Y.J., 0000-0002-2745-4323; T.A.S., 0000-0001-6627-2904; W.P.W., 0000-0001-7398-546X

References

1 Sadler, J. E. Biochemistry and genetics of von Willebrand factor. *Annu. Rev. Biochem.* **67**, 395-424 (1998).

2 Springer, T. von Willebrand factor, Jedi knight of the bloodstream. *Blood* **124**, 1412-1425 (2014).

3 Sadler, J. E. New concepts in von Willebrand disease. *Annu Rev Med* **56**, 173-191 (2005).

4 Savage, B., Almus-Jacobs, F. & Ruggeri, Z. M. Specific synergy of multiple substrate-receptor interactions in platelet thrombus formation under flow. *Cell* **94**, 657-666 (1998).

5 Reininger, A. J. Function of von Willebrand factor in haemostasis and thrombosis. *Haemophilia* **14 Suppl 5**, 11-26 (2008).

6 Fu, H. *et al.* Flow-induced elongation of von Willebrand factor precedes tension-dependent activation. *Nat Commun* **8**, 324, doi:10.1038/s41467-017-00230-2 (2017).

7 Jiang, Y., Fu, H., Springer, T. A. & Wong, W. P. Electrostatic Steering Enables Flow-Activated Von Willebrand Factor to Bind Platelet Glycoprotein, Revealed by Single-Molecule Stretching and Imaging. *J Mol Biol* **431**, 1380-1396, doi:10.1016/j.jmb.2019.02.014 (2019).

8 Savage, B., Sixma, J. J. & Ruggeri, Z. M. Functional self-association of von Willebrand factor during platelet adhesion under flow. *Proc Natl Acad Sci U S A* **99**, 425-430 (2002).

9 Shankaran, H., Alexandridis, P. & Neelamegham, S. Aspects of hydrodynamic shear regulating shear-induced platelet activation and self-association of von Willebrand factor in suspension. *Blood* **101**, 2637-2645 (2003).

10 Ulrichts, H. *et al.* The von Willebrand factor self-association is modulated by a multiple domain interaction. *J Thromb Haemost* **3**, 552-561, doi:JTH1209 [pii] 10.1111/j.1538-7836.2005.01209.x (2005).

11 Barg, A. *et al.* Soluble plasma-derived von Willebrand factor assembles to a haemostatically active filamentous network. *Thromb Haemost* **97**, 514-526 (2007).

12 Dayananda, K. M., Singh, I., Mondal, N. & Neelamegham, S. von Willebrand factor self-association on platelet GpIbα under hydrodynamic shear: effect on shear-induced platelet activation. *Blood* **116**, 3990-3998, doi:10.1182/blood-2010-02-269266 (2010).

13 Chung, D. W. *et al.* High-density lipoprotein modulates thrombosis by preventing von Willebrand factor self-association and subsequent platelet adhesion. *Blood* **127**, 637-645, doi:10.1182/blood-2014-09-599530 (2016).

14 Zhang, C., Kelkar, A. & Neelamegham, S. von Willebrand factor self-association is regulated by the shear-dependent unfolding of the A2 domain. *Blood Adv* **3**, 957-968, doi:10.1182/bloodadvances.2018030122 (2019).

15 Yuan, H. *et al.* The unfolded von Willebrand factor response in bloodstream: the self-association perspective. *J Hematol Oncol* **5**, 65, doi:10.1186/1756-8722-5-65 (2012).

16 Lopez, J. A. & Chung, D. W. VWF self-association: more bands for the buck. *Blood* **116**, 3693-3694, doi:10.1182/blood-2010-09-303438 (2010).

17 Blenner, M. A., Dong, X. & Springer, T. A. Structural basis of regulation of von Willebrand factor binding to glycoprotein Ib. *J. Biol. Chem.* **289**, 5565-5579, doi:M113.511220 [pii] 10.1074/jbc.M113.511220 (2014).

18 Handin, R. I., Lux, S. E. & Stossel, T. P. *Blood: principles and practice of hematology*. Second edn, (Lippincott Williams & Wilkins, 2003).

19 Huang, R. H., Fremont, D. H., Diener, J. L., Schaub, R. G. & Sadler, J. E. A structural explanation for the antithrombotic activity of ARC1172, a DNA aptamer that binds von Willebrand factor domain A1. *Structure* **17**, 1476-1484, doi:10.1016/j.str.2009.09.011 (2009).

20 Diener, J. L. *et al.* Inhibition of von Willebrand factor-mediated platelet activation and thrombosis by the anti-von Willebrand factor A1-domain aptamer ARC1779. *J Thromb Haemost* **7**, 1155-1162, doi:10.1111/j.1538-7836.2009.03459.x (2009).

21 Parker, E. T. & Lollar, P. Conformation of the von Willebrand factor/factor VIII complex in quasi-static flow. *J Biol Chem* **296**, 100420, doi:10.1016/j.jbc.2021.100420 (2021).

22 Kim, J., Zhang, C. Z., Zhang, X. & Springer, T. A. A mechanically stabilized receptor-ligand flex-bond important in the vasculature. *Nature* **466**, 992-995, doi:10.1038/nature09295 (2010).

23 Ju, L., Dong, J. F., Cruz, M. A. & Zhu, C. The N-terminal flanking region of the A1 domain regulates the force-dependent binding of von Willebrand factor to platelet glycoprotein Ibα *J Biol Chem* **288**, 32289-32301, doi:10.1074/jbc.M113.504001 (2013).

24 Zhang, X., Halvorsen, K., Zhang, C. Z., Wong, W. P. & Springer, T. A. Mechanoenzymatic cleavage of the ultralarge vascular protein, von Willebrand factor. *Science* **324**, 1330-1334 (2009).

25 Ying, J., Ling, Y., Westfield, L. A., Sadler, J. E. & Shao, J. Y. Unfolding the A2 domain of von Willebrand factor with the optical trap. *Biophys J* **98**, 1685-1693, doi:S0006-3495(10)00096-2 [pii] 10.1016/j.bpj.2009.12.4324 (2010).

26 Wu, T., Lin, J., Cruz, M. A., Dong, J. F. & Zhu, C. Force-induced cleavage of single VWF A1A2A3-tridomains by ADAMTS-13. *Blood* **115**, 370-378, doi:blood-2009-03-210369 [pii] 10.1182/blood-2009-03-210369 (2010).

27 Evans, E. & Ritchie, K. Dynamic strength of molecular adhesion bonds. *Biophys. J.* **72**, 1541-1555 (1997).

28 Dudko, O. K., Hummer, G. & Szabo, A. Intrinsic rates and activation free energies from single-molecule pulling experiments. *Phys. Rev. Lett.* **96**, 108101-108104 (2006).

29 Astrof, N. S., Salas, A., Shimaoka, M., Chen, J. F. & Springer, T. A. Importance of force linkage in mechanochemistry of adhesion receptors. *Biochemistry* **45**, 15020-15028 (2006).

30 Springer, T. A. Structural basis for selectin mechanochemistry. *Proc. Natl. Acad. Sci. U. S. A.* **106**, 91-96 (2009).

31 Yakovenko, O. T., V.; Sokurenko, E.V.; Thomas, W.E.. Inactive conformation enhances binding function in physiological conditions. *Proc Natl Acad Sci USA.* **112**, 9884-9889, doi:10.1073/pnas.1503160112 (2015).

Figure Legends

Figure 1. **Association of VWF in flow to tethered VWF. (A)** Schematic of TIRF microscopy with air pressure-actuated flow. **(B)** Dual-color fluorescence images showing the extension and relaxation of a representative tethered Alexa 488-labeled VWF molecule and the binding and dissociation of Alexa 647-labeled VWF in flow at the indicated wall shear stresses. **(C)** Average time course of free VWF association to single tethered VWF concatemers. The Y axis is the mass ratio of bound VWF / tethered VWF. The red triangle marks the increase in flow from 80 dyn cm^{-2} to the shear rate keyed by color and black triangles mark resumption of flow at 80 dyn cm^{-2}. **(D)** Profile of final VWF binding density at relative locations along individual tethered VWF concatemers. $N_{freeVWF}$ is the monomer number of bound VWF **(E)** Dissociation rate at 80 dyn cm^{-2} of VWF that had been bound at different wall shear stresses. Dissociation in **(C)** was fit to a double exponential function

$$R_{freeVWF}(t) = R_{freeVWF,fast} \cdot \exp(-k_{off,fast} \cdot t) + R_{freeVWF,slow} \cdot \exp(-k_{off,slow} \cdot t).$$

In **C**-**E**, binding of free VWF (10 μg mL^{-1}) was measured on N = 93 tethered VWF molecules. The average end-to-end distance of these VWF molecules was 3.6±1.1 μm at 960 dyn cm^{-2}, and they contained 149±32 monomers based on integrated fluorescence intensity.

Figure 2. Tension-regulated VWF self-association. (A) Average time course of VWF (10 μg mL^{-1}) binding to single tethered VWF concatemers at 960 dyn cm^{-2}. Curves show association (solid lines) and dissociation at 80 dyn cm^{-2} (dashed lines) and are color coded by tension bin as shown in the key (the triangle shows the tether point). Data are averaged from N = 62 tethered VWF molecules used in Figure **1C**-**E** that are large enough to include a 40-60 pN tension bin at 960 dyn cm^{-2}. **(B)** Initial VWF binding rate and **(C)** final bound density of VWF from data in **A**. In **B** and **C**, the maximum binding rate and total binding density are estimated as the average of the values in the 20-30 and 30-40 pN bins. The force at half-maximal binding, f_{50}, was determined as the intercept of the half maxima with the lines drawn through the data points on either side of the half-maxima. **(D)** Initial binding rate of VWF (10 μg mL^{-1}) at 480 dyn cm^{-2} using smaller (5 pN) tension bins. In **B**-**D**, red lines connect neighboring points. **(E-F)** Fits of the data in **B** and **D** to a two-state model (red lines) in which the observed initial binding rate $k_{obs} = k_{obs,max}/(1 + \exp((\Delta G - f \cdot \Delta x)/k_B T))$, where $k_{obs,max}$ is the maximum observed initial binding rate, ΔG is the free energy difference between the two states (fast binding and slow or no binding), and Δx is the displacement along the force f direction between the two states. Data in **A**-**F** are from the same set of tethered VWF concatemers. In **B**-**D**, error bars are standard deviation. In **E**-**F**, error bars are standard deviation for tension and 95% confidence intervals for the other variables.

Figure 3. VWF self-association kinetics as a function of free VWF concentration and shear stress. (A) Scheme for VWF self-association. Upper: A primary VWF molecule tethered on the substrate at the large open triangle is shown with secondary VWF molecules tethered at small closed triangles. Lower: Key for the tension within each VWF molecule. **(B)** Average time course of VWF self-association following wall shear stress increase from 80 to 240, 480, or 960 dyn cm^{-2} (red arrows) and then decrease to 80 dyn cm^{-2} (black arrows) with 1, 5, 10, 50 μg mL^{-1} free VWF. Different sets of tethered VWF molecules (in independent flow channels) were measured for each free VWF concentration; at each free VWF concentration, the same set of tethered VWF molecules was measured at each shear stress. Data were from N=67, 70, 93, 57 VWF molecules for 1, 5, 10, 50 μg mL^{-1} free VWF, respectively. Data for 10 μg mL^{-1} free VWF are the same as in Figure 1C. Flow pattern, imaging exposure time, and frame rates are described in Supplemental Tables 1 and 2.

Figure 4. Dependence of VWF self-association on free VWF concentration. **(A)** Free VWF binding kinetics (solid lines) after flow increase from 80 to 960 dyn cm^{-2} at different concentrations of free VWF. For each tension bin, the curves were fitted using a homogeneous binding model assuming the free VWF binds as individual monomers. Fitting to the following equation yielded the dissociation and association rate (k_{off} and k_{on}) for free VWF binding to regions of tethered VWF [6].

$$=N_{total} \cdot (1\text{-}\exp(-(k_{on}[C] + k_{off})\Delta t \cdot i)) \cdot k_{on}[C]/(k_{on}[C] + k_{off})$$

where N_{total} is the total number of binding sites in tethered VWF that belong to the tension bin, $N_{freeVWF}$ is the monomer number of bound VWF in the same region, [C] is the concentration of free VWF monomers in solution, i is the frame number, and Δt is the time lag between consecutive frames. The predictions of the fitted model are shown in corresponding colors (dashed lines). Data for 1, 5, 10, and 50 μg mL^{-1} free VWF are with 52, 69, 62, and 51 tethered VWF concatemers, respectively, which were long enough to include a 40-60 pN tension bin. Data for 10 μg mL^{-1} free VWF are the same as in Figure 3. **(B)** Initial VWF binding rate per μm of tethered VWF in each tension bin at 960 dyn cm^{-2} wall shear stress (circles). The data points corresponding to the tension bins are jittered along the X-axis to avoid overlap. Dashed lines show linear fit (inset formula) to the data points from 1-10 μg mL^{-1} VWF, i.e with data at 50 μg mL^{-1} VWF omitted from the fit (see Results). a(f) is a tension-dependent, numerical fitting parameter. **(C)** Tension dependence of the a(f) value determined in **(B)**. Red lines connect points.

Figure 5. Effect of VWF self-association on GPIbα binding. (A) Time course of GPIbα647 binding to Alexa Fluor 488-labeled tethered VWF in the presence of 20 nM GPIbα647 and 0, 10, or 50 μg mL^{-1} of free unlabeled VWF at 960 dyn cm^{-2} wall shear stress. Tension bins are keyed according to color. **(B-C)** Number of bound GPIbα647 averaged over time periods between 1.5-2.5 s **(B)** and 27-35 s **(C)** after the start of flow at 960 dyn cm^{-2}. Data for 0, 10, and 50 μg mL^{-1} of free VWF are averages over 48, 170, and 166 tethered VWF concatemers, respectively.

522 **Figure 1.**

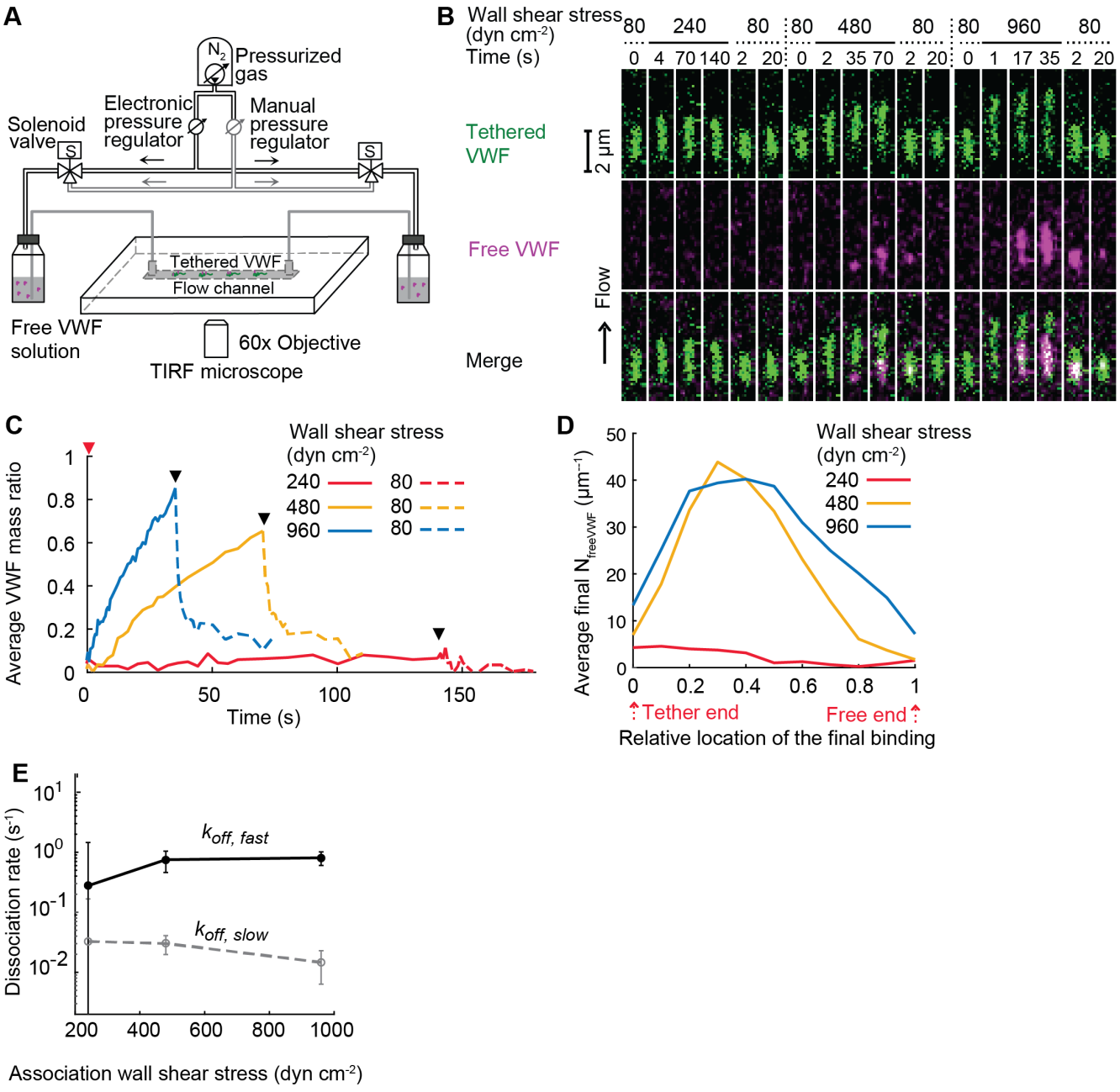

523

524 **Figure 2.**

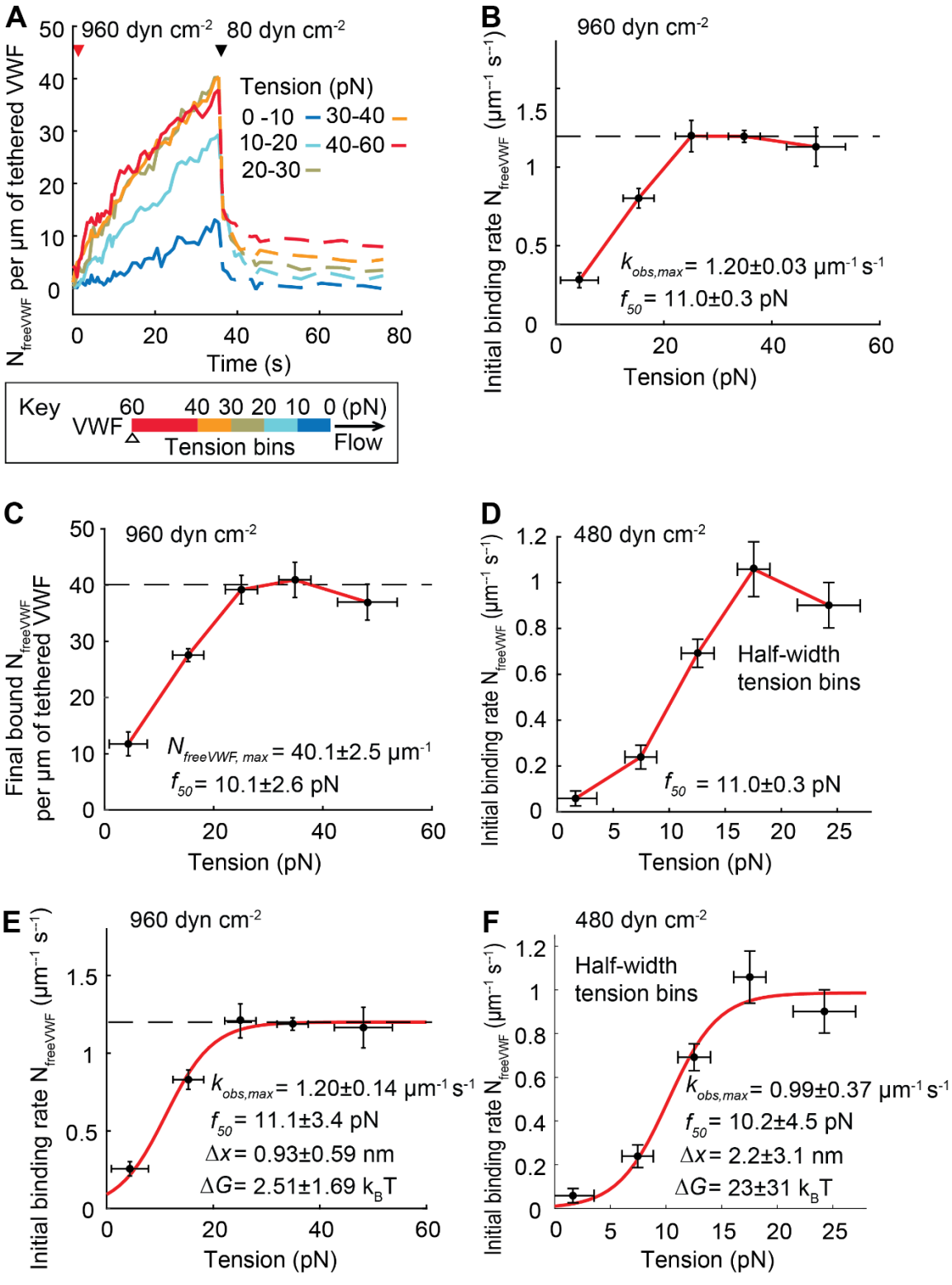

525
526

527 **Figure 3.**

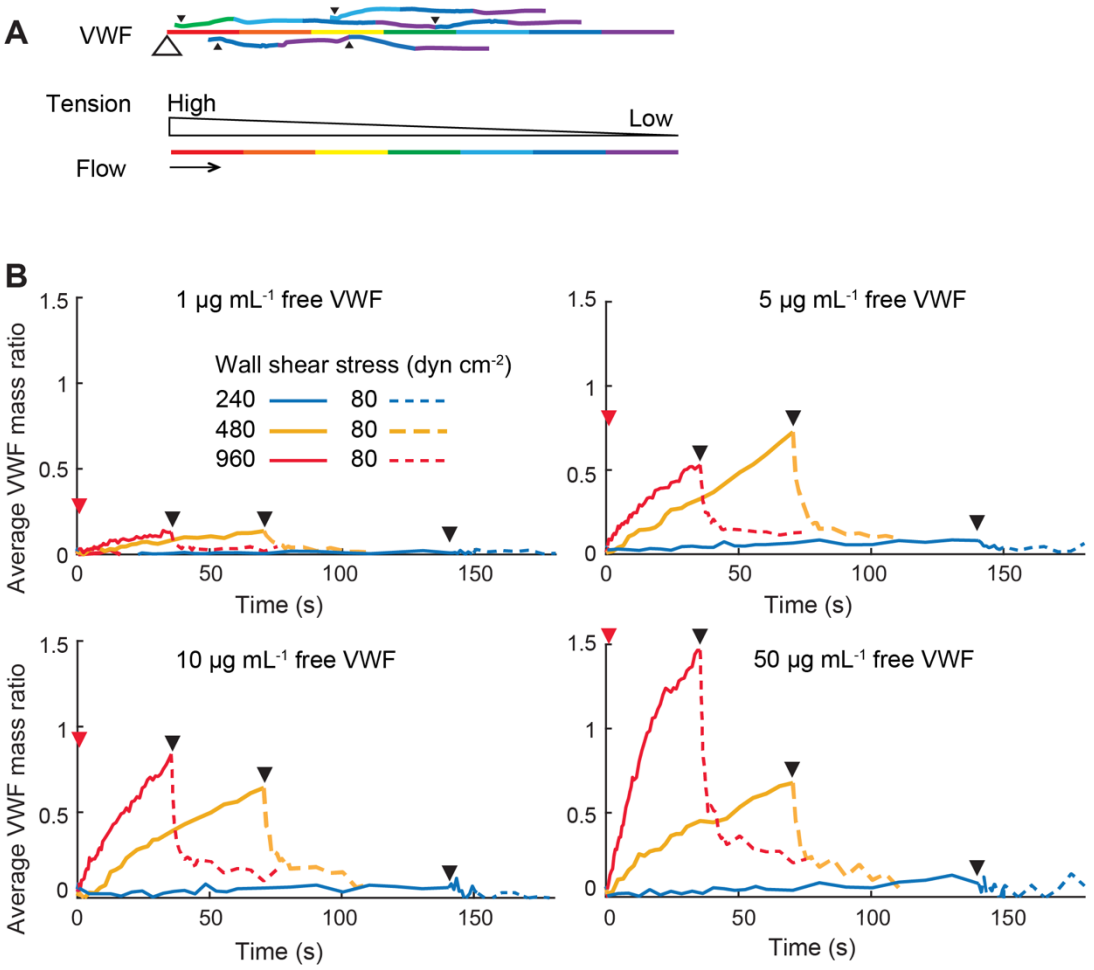

528

Figure 4.

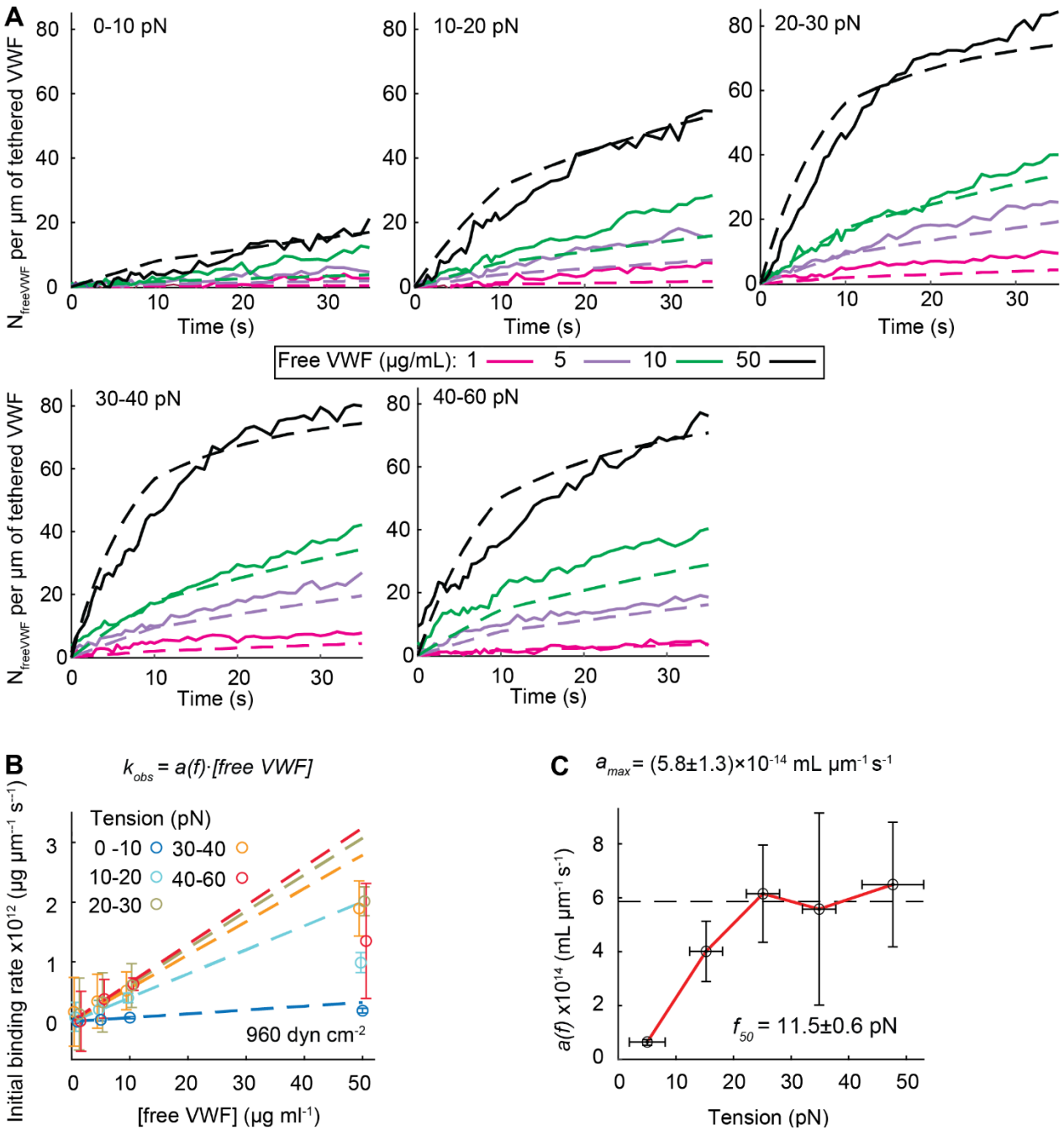
A
0-10 pN
10-20 pN
20-30 pN
30-40 pN
40-60 pN
N_freeVWF per µm of tethered VWF
Time (s)
Free VWF (µg/mL): 1 5 10 50
B
k_obs = a(f)·[free VWF]
Tension (pN)
0 -10
10-20
20-30
30-40
40-60
960 dyn cm-2
Initial binding rate x10^12 (µg µm^-1 s^-1)
[free VWF] (µg ml^-1)
C
a_max = (5.8±1.3)×10^-14 mL µm^-1 s^-1
a(f) x10^14 (mL µm^-1 s^-1)
f_50 = 11.5±0.6 pN
Tension (pN)

Figure 5.

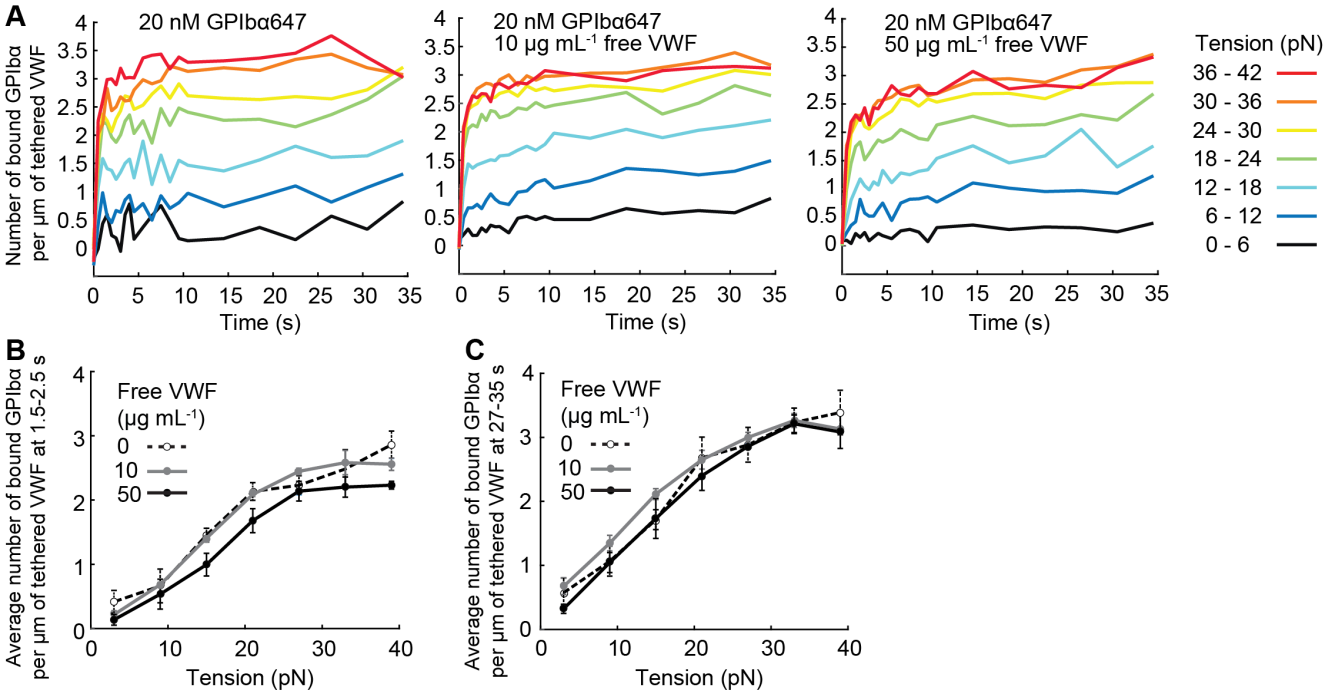
A
20 nM GPIbα647
20 nM GPIbα647
10 μg mL-1 free VWF
20 nM GPIbα647
50 μg mL-1 free VWF
Number of bound GPIbα per μm of tethered VWF
Time (s)
Tension (pN)
36 - 42
30 - 36
24 - 30
18 - 24
12 - 18
6 - 12
0 - 6
B
Average number of bound GPIbα per μm of tethered VWF at 1.5-2.5 s
Free VWF (μg mL-1)
0
10
50
Tension (pN)
C
Average number of bound GPIbα per μm of tethered VWF at 27-35 s
Free VWF (μg mL-1)
0
10
50
Tension (pN)

Supplemental Data

Supplemental Methods

Recombinant VWF and GPIbα. Recombinant human wild-type VWF[1] (Baxter BioScience, Vienna, Austria) was labeled with Alexa Fluor 488 (Thermo Fisher Scientific) (degree of labeling: 1.80 fluorophores per VWF monomer) and biotin (~ 0.3 biotin or twin-biotin molecules per VWF monomer, using sulfosuccinimidyl-6-[biotin-amido] hexanoate (EZ-link Sulfo-NHS-LC-Biotin, Thermo Fisher Scientific)), or TFP-dPEG®4-Lys-(dPEG®4-biotin)2 (Quanta BioDesign, Ltd) with twin-biotin for strong tethering between VWF and surface). After size fractionation using Sepharose CL-2B (Pharmacia Fine Chemicals, Sweden), VWF molecules with a median size of ~ 40 monomers per concatemer were used as tethered VWF [2]. For use as free VWF in the fluid phase, VWF was labeled with Alexa Fluor 647 (Thermo Fisher Scientific) (1.42 fluorophores per monomer), dialyzed to remove the free fluorescent dye, and used without size fractionation.

Recombinant human platelet GPIbα (His^{1} to Arg^{290}) containing platelet-type von Willebrand disease (PT-VWD) mutations G233V and M239V was conjugated with Alexa Fluor 647 as described (2.34 fluorophores per molecule)[2-4]. Cell lines were confirmed as mycoplasma free using a mycoplasma detection kit (Lonza Biologics). VWF and GPIbα samples were aliquoted and stored at -80 °C.

Dual-color TIRF and microfluidics. To construct the microfluidic flow channel, low-density biotin-PEG/PEG-coated #1.5 cover glass (Bio 01, MicroSurfaces, Englewood, NJ, USA) was overlaid with a central piece of ~ 100 μm thick, double-sided Kapton polyimide tape with 0.5 mm × 15 mm cutouts and topped with a 1.1 mm thick glass slide with two access holes for each channel. A ~3 mm thick polydimethylsiloxane (PDMS) slab with 0.75 mm diameter holes was aligned with the access holes and clamped onto the glass sandwich. The holes on each end of the flow channel were connected through 1/32" outer diameter PEEK tubing (1569, IDEX Health & Science, Middleborough, MA, USA) to ~ 1 ml of buffer in a 4 ml gas tight vial containing nitrogen gas (Fig. 1b). Each vial was further connected to a three-way solenoid valve (411L3312HV, ASCO Valve, Fort Mill, SC, USA) to rapidly switch the gas between the baseline pressure and high pressures to control the flow rate. The baseline and high pressures were respectively supplied by a manual pressure

regulator (30222-Z21958, Fairchild) and a high-precision electronic pressure regulator (DQPV1TFEE010CXL, Proportion-Air) connected to compressed nitrogen cylinder (>99% pure, Lifegas, Marlborough, MA, USA).

Wall shear rate was calculated from the volumetric flow rate and the height and width of the flow channel[5]. The volumetric flow rate was measured by weighing the buffer bottle before and after 15-30 s of buffer flow driven at 1.2, 3, and 6 psi. As expected, the volumetric flow rate was approximately proportional to pressure. The measured slope of the linear relation was used to calculate the flow driving pressure to attain any given shear rate.

We used a dual-color TIRF microscope built on a vibration damping optical table (RS4000, Newport, Irvine, CA, USA) with a 60x oil TIRF objective (NA 1.49, CFI Apo TIRF 60x H, Nikon, Japan), 485 nm laser (CUBE 485-30C, Coherent, Santa Clara, CA, USA), 642 nm laser (DL640-050, Crystalaser, Reno, NV, USA) with a rotating diffuser, an EMCCD camera (DU-897, Andor, UK) for the 485nm channel and an EMCCD camera (C9100, Hamamatsu, Japan) for the 642nm channel. Synchronized image recording and flow was controlled with custom software (LabView, National Instruments, Austin, TX, USA).

Experimental procedures. A mixture (1:1) of BSA (BSA-Block, Candor Bioscience GmbH) and casein (The Blocking Solution, Candor Bioscience GmbH) was incubated in a flow channel for 30 min to block the non-specific binding of the surface. To tether VWF molecules on the channel surface, the channel was incubated with traptavidin[6] (Kerafast Inc., 0.2 μg mL^{-1}), a mechanically stable streptavidin, for 10 min to allow binding to biotin-PEG on the surface. The channel was then washed with wash buffer (150 mM NaCl, 20 mM HEPES pH 7.4), and incubated with biotin- and Alexa Fluor 488-labeled VWF concatemers (1 μg mL^{-1}) for 10 min. The channel was then incubated with D-biotin (5 mM) for 20 min to block extra traptavidins on the surface. After washing with wash buffer, the channel was ready for use.

In experiments, an imaging buffer containing free VWF and/or GPIbα was added to the gas-tight vials and flowed through the channel at different flow rates and directions. The imaging buffer contained 150 mM NaCl, 20 mM HEPES (pH 7.4), 0.02% Tween 20, 0.1 mM D-biotin (Invitrogen), 0.5 mg/mL BSA, 2.2 mM

protocatechuic acid (PCA) (Santa Cruz Biotechnology) and 37 nM protocatechuate-3,4-dioxygenase (PCD) (Sigma-Aldrich) as oxygen scavengers[7]. Experiments were at 21°C.

To measure free VWF binding to tethered VWF molecules, the flow sequences in Supplemental Table 1 and the imaging exposure time and frame rates in Supplemental Table 2 were used. Within our experimental time window, binding of free VWF to tethered VWF was not detected at 0-80 dyn cm^{-2}. Free VWF in solution diffuses and creates a non-uniform fluorescence background at 0 dyn cm^{-2}. At 80 dyn cm^{-2}, the fluorescence background is more uniform and was subtracted from images at higher shear.

To measure GPIbα binding to Alexa Fluor 488-labeled tethered VWF molecules, 20 nM Alexa647-GPIbα with 0, 10, or 50 μg mL^{-1} of free unlabeled VWF was perfused at 960 dyn cm^{-2} wall shear stress for 35 s in the flow channel and fluorescence at stasis was subtracted as the baseline. Fluorescence images were collected with 10 ms exposure time at 2 frames per second (fps).

For inhibition by GPIbα (200 nM) and the aptamer ARC1172 (60 nM) of VWF self-association, 10 μg mL^{-1} Alexa Fluor 647-labeled free VWF was perfused at 960 dyn cm^{-2} wall shear stress for 35 s.

Data analysis. Fluorescence was analyzed with custom-written Matlab scripts. Registration mapping between Alexa Fluor 488 and Alexa Fluor 647 images used slides with multicolor 100 nm TetraSpeck microsphere (Thermo Fisher Scientific) fiducials that were excited and detected in the corresponding channels. Alexa Fluor 647 images were transformed according to the registration mapping to match the Alexa Fluor 488 images. Rectangular regions of interest (ROI) for individual VWF molecules were initially defined manually based on background-subtracted Alexa Fluor 488 images. Thresholding and particle analysis were then used to determine the contours of individual VWF molecules to refine ROIs. Length and intensity profiles of VWF and bound GPIbα were then calculated. Average intensity of single Alexa Fluor 488 or Alexa Fluor 647 fluorophores was measured by stepwise photobleaching of Alexa Fluor 488 dye-labeled streptavidin or Alexa Fluor 647 dye-labeled GPIbα sparsely attached on the glass surface. The number of VWF monomers or GPIbα molecules was determined by the total fluorescence intensity of VWF or GPIbα divided by the corresponding single Alexa Fluor dye intensity and their respective degree of labeling (0.67:1 for VWF and 1.01:1 for GPIbα).

While single dye standards were attached to the surface, VWF and GPIbα bound to VWF in flow experiments could be more distal from the surface, which would decrease their fluorescence intensity in the TIRF evanescent illumination by an unknown amount, for which we did not correct. As described below, the average height of VWF was estimated to be 10-20 nm above the substrate. The average height of dyes on streptavidin were estimated to be 4.5 nm (2 × 1 nm for the two biotins + 5 nm for the traptavidin / 2) above the substrate. Assuming a penetration depth of 150 nm for the evanescent illumination, we estimated the ratio of illumination intensity for dyes on VWF to dyes on streptavidin to be 0.96-0.9. These estimates suggest that the correction would be small. The number of monomers in individual VWF concatemers was estimated using the total Alexa Fluor 488 fluorescence intensity of VWF divided by the degree of labeling and the intensity of single Alexa Fluor 488 fluorophores. The mass of each VWF molecule was calculated from the mass of VWF monomers multiplied by the total monomer number in that molecule. The number of GPIbα was determined by the total fluorescence intensity of GPIbα divided by the single Alexa Fluor 647 intensity and the degree of labeling.

For each tethered VWF, the final binding intensity profile was calculated as the average of the 120-140, 60-70, and 33-35 second time interval after the increase of flow to 240, 480, and 960 dyn cm^{-2}, respectively. Dissociation rates were calculated from averaged intensity traces after the decrease of shear to 80 dyn cm^{-2}.

Tension along each tethered VWF was estimated as described in [2]. Briefly, the tension in tethered VWF was estimated as the sum of drag forces on the downstream monomers. The drag force on each VWF monomer is proportional to the wall shear stress and is 0.38 and 0.19 pN at 960 and 480 dyn cm^{-2}, respectively. The fluorescent intensity profile of the tethered VWF during the first 3 seconds after the start of flow was used to calculate the number of monomers in that molecule. Free VWF molecules bound from the flow stream likely add additional drag force on tethered VWF. Higher tension and higher free VWF concentration might induce more binding and more increase of tension. However, the wide size range of VWF in the flow stream and lack of knowledge about the binding sites for each bound VWF molecule on tethered VWF prevented meaningful

calculation of their effects on the resulting distribution of tensile force in tethered VWF. Therefore, we did not include the effect of bound VWF on our tension calculation and instead used the pre-association tension profile.

To analyze binding kinetics as a function of tension, the average fluorescence intensity of bound VWF under 960 or 480 dyn cm^{-2} flow was averaged within each tension bin along the extended tethered VWF molecules. At 80 dyn cm^{-2} flow, tethered single VWF molecules were shorter than at 960 or 480 dyn cm^{-2}. Therefore, the tension bins defined at 960 or 480 dyn cm^{-2} flow were mapped onto the less extended VWF molecule using a length scaling factor of 0.4 or 0.5, respectively. The scaling factors were calculated from the average curve for VWF extension vs. shear stress measured previously[2]. For the 960 dyn cm^{-2} experiments, the observed initial binding rate of free VWF in each tension bin was calculated as the slope of the linear region, specifically the first 35, 20, 10, or 3 seconds, of each binding curve after the increase of flow for 1, 5, 10, and 50 μg mL^{-1} free VWF, respectively. Final binding $N_{freeVWF}$ was the average of the 33-35 second binding curve within each tension bin after the increase of flow to 960 dyn cm^{-2}. Tension f_{50} at the half maximum was linearly interpolated from the two nearest data points whose y values bracketed the half maximum. For the 10 μg mL^{-1} free VWF experiments at 480 dyn cm^{-2}, the observed initial binding rate was calculated as the slope of the first 5 seconds of the binding curve after the increase of flow. To measure the tension dependence of GPIbα binding to tethered VWF in the presence of 0, 1, 10, or 50 μg mL^{-1} free VWF, we calculated the average bound GPIbα fluorescence intensity within each tension bin at 960 dyn cm^{-2}.

We included all elongated tethered VWF molecules in our data analysis except for molecules with mass ratios of pre-bound free VWF to tethered VWF greater than 0.2 before the increase of flow from 80 dyn cm^{-2}. Such associations likely arose during previous experiments and did not fully dissociate.

Code availability. Custom-written MATLAB codes for data analysis are available from the corresponding authors upon request.

Statistical analysis. The sample size was not predetermined. Experiments were repeated in different flow channels 2-3 times and these results were pooled together and averaged in the data presented.

Supplemental Table 1. Standard flow sequence for VWF self-association

Wall shear stress (dyn cm^{-2})	80	240	80	480	80	960	80
Dwell time (s)	1	140	41	70	41	35	40
Elapsing time (s)	0-1	2-142	143-184	185-255	256-297	298-333	334-374

Supplemental Table 2. Imaging exposure times and frame rates for VWF self-association

Wall shear stress (dyn cm^{-2})	240*		480*		960*	
	Elapsing time (s)	Frame rate (fps)	Elapsing time (s)	Frame rate (fps)	Elapsing time (s)	Frame rate (fps)
Pre-period at 80 dyn cm^{-2}	0-1	2	0-1	2	0-1	2
Initial association	0-60	0.25	0-30	0.5	0-10	2
Later association	60-140	0.1	30-70	0.2	10-35	1
Initial dissociation at 80 dyn cm^{-2}	0-10	1	0-10	1	0-10	1
Later dissociation at 80 dyn cm^{-2}	10-40	0.2	10-40	0.2	10-40	0.2

* Exposure times: 0.007, 0.008, and 0.008 s at wall shear stresses of 240, 480, and 960 dyn cm^{-2}, respectively.

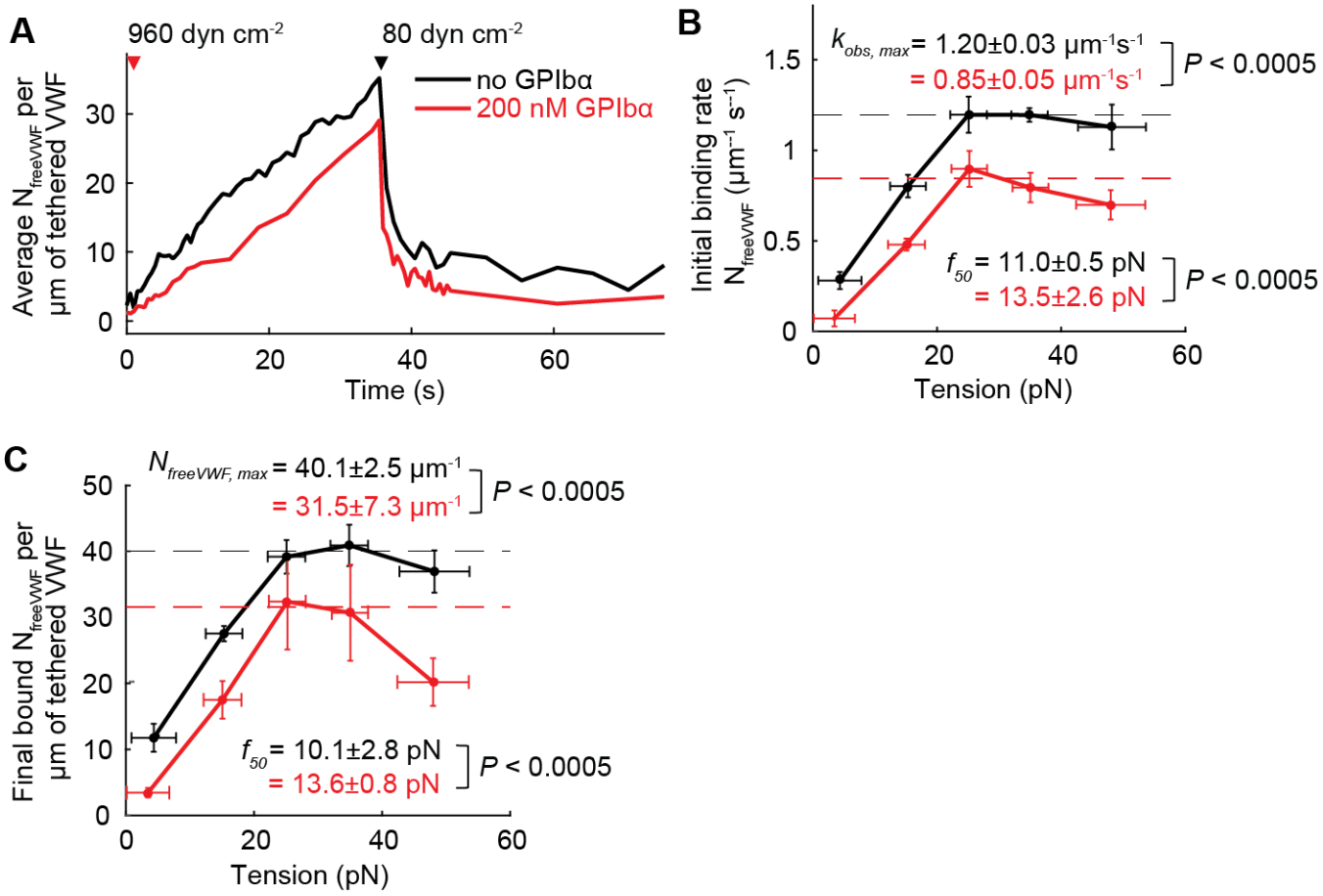

Supplemental Figure 1. Effects of GPIbα binding on VWF self-association. (A) Time course of VWF self-association in the presence of 10 µg mL^{-1} of Alexa Fluor 647-labeled free VWF, 0 (black) or 200 (red) nM unlabeled GPIbα following shear stress increasing from 80 to 960 dyn cm^{-2} (red arrow) and then decreasing to 80 dyn cm^{-2} (black arrow). *N* = 119 VWF concatemers. We used 10 µg mL^{-1} free VWF, which approximates the normal blood concentration, and 200 nM GPIbα, which is more than twice the VWF-GPIbα binding affinity value under tension activated conditions (> 24 pN) [2]. **(B)** Average observed initial binding rate and **(C)** final binding of free VWF ($N_{freeVWF}$) v.s. tension. Tension bins are the same as in Figure 2A. Black/red dashed lines indicate the maximum observed binding rate $k_{obs,max}$ and maximum final bound $N_{freeVWF,max}$ of free VWF, in the presence of 0/200 nM GPIbα, respectively. f_{50} is the interpolated tension at the half of $k_{obs,max}$ and $N_{freeVWF,max}$. *p* value is <0.0005 in **(B).** p value is 0.0051, 0.0073, 0.18, 0.082, and 0.0061 for the tension bins 0-10, 10-20, 20-30, 30-40, and 40-60 pN in **(C)**, respectively.

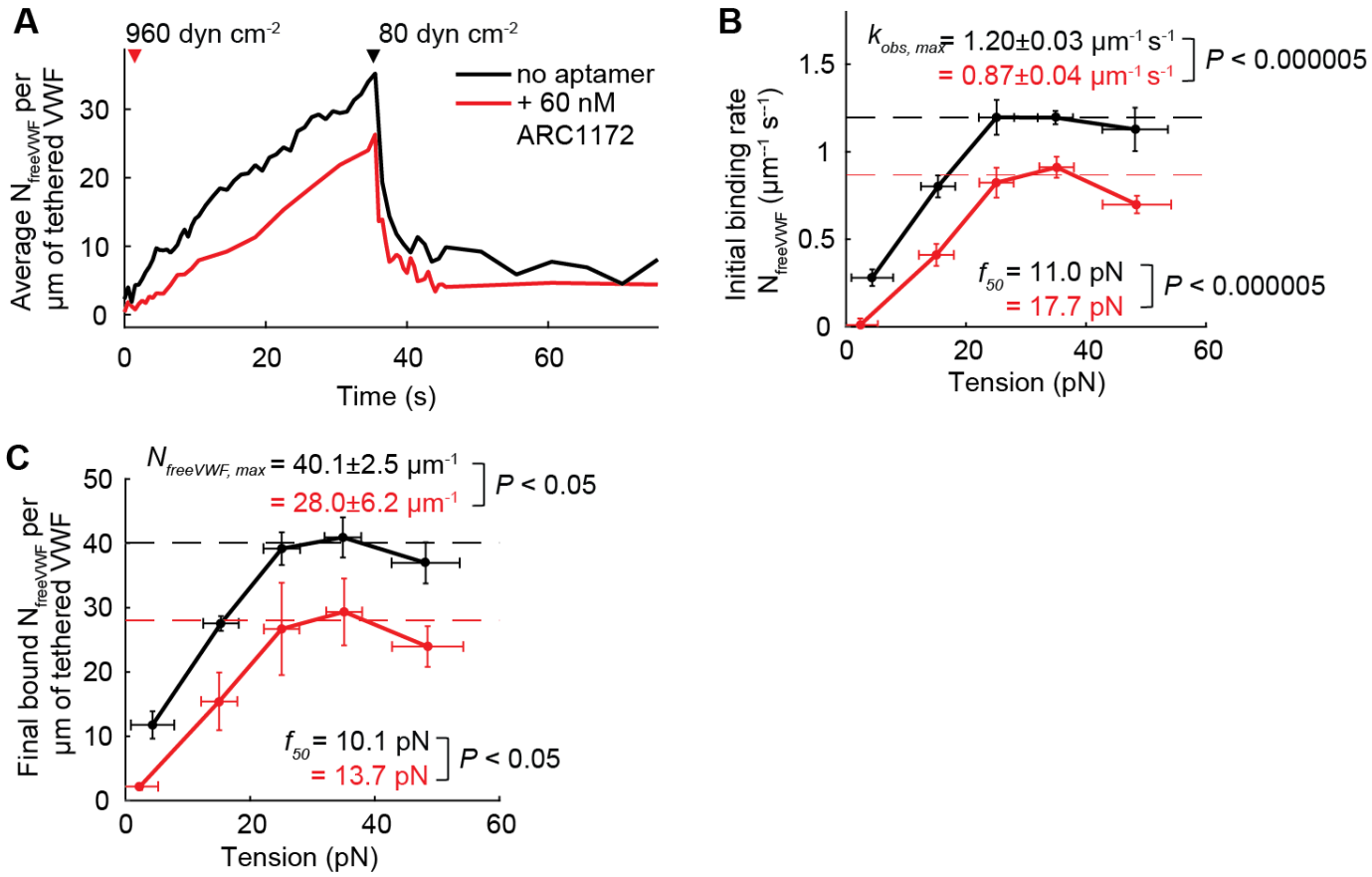

Supplemental Figure 2. Effects of A1 aptamer on VWF self-association. (A) Time course of VWF self-association in the presence of 10 µg mL^{-1} of Alexa Fluor 647-labeled free VWF, and 0 (black) or 60 nM (red) unlabeled A1 aptamer ARC1172 flowing shear stress increasing from 80 to 960 dyn cm^{-2} (red arrow) and then decreasing to 80 dyn cm^{-2} (black arrow). N = 98 VWF concatemers. **(B)** Average observed initial binding rate of free VWF and **(C)** final $N_{freeVWF}$ v.s. tension. Tension bins are the same as in Figure 2A. Black/red dashed lines indicate the maximum observed binding rate $k_{obs,max}$ and maximum final bound $N_{freeVWF,max}$ of free VWF, in the presence of 0/60 nM ARC1172, respectively. f_{50} is the interpolated tension at the half of $k_{obs,max}$ and $N_{freeVWF,max}$. p value is <0.000005 in **(B)**, and <0.05 in **(C)**.

References:

1 Turecek, P. L. *et al.* Development of a plasma- and albumin-free recombinant von Willebrand factor. *Hamostaseologie* **Suppl 1**, S32-38 (2009).

2 Fu, H. *et al.* Flow-induced elongation of von Willebrand factor precedes tension-dependent activation. *Nat Commun* **8**, 324, doi:10.1038/s41467-017-00230-2 (2017).

3 Blenner, M. A., Dong, X. & Springer, T. A. Structural basis of regulation of von Willebrand factor binding to glycoprotein Ib. *J. Biol. Chem.* **289**, 5565-5579, doi:M113.511220 [pii] 10.1074/jbc.M113.511220 (2014).

4 Jiang, Y., Fu, H., Springer, T. A. & Wong, W. P. Electrostatic Steering Enables Flow-Activated Von Willebrand Factor to Bind Platelet Glycoprotein, Revealed by Single-Molecule Stretching and Imaging. *J Mol Biol*, doi:10.1016/j.jmb.2019.02.014 (2019).

5 Son, Y. Determination of shear viscosity and shear rate from pressure drop and flow rate relationship in a rectangular channel. *Polymer* **48**, 632-637, doi:10.1016/j.polymer.2006.11.048 (2007).

6 Chivers, C. E. *et al.* A streptavidin variant with slower biotin dissociation and increased mechanostability. *Nat Methods* **7**, 391-393, doi:10.1038/nmeth.1450 (2010).

7 Aitken, C. E., Marshall, R. A. & Puglisi, J. D. An oxygen scavenging system for improvement of dye stability in single-molecule fluorescence experiments. *Biophys J* **94**, 1826-1835, doi:10.1529/biophysj.107.117689 (2008).

VWF self-association in high shear

Primary tethered VWF molecule,
with tension applied by hydrodynamic drag

Secondary VWF molecule bound from
the flow stream to tension-activated sites

Dissociation in low shear

Key

Tension High Low

Flow